

Lawrence Berkeley National Laboratory

LBL Publications

Title

Advanced control strategies to manage electric vehicle drivetrain battery health for Vehicle-to-X applications

Permalink

<https://escholarship.org/uc/item/0472k7qh>

Authors

Gehbauer, Christoph

Black, Douglas R

Grant, Peter

Publication Date

2023-09-01

DOI

10.1016/j.apenergy.2023.121296

Copyright Information

This work is made available under the terms of a Creative Commons Attribution-NonCommercial License, available at <https://creativecommons.org/licenses/by-nc/4.0/>

Peer reviewed



Advanced control strategies to manage electric vehicle drivetrain battery health for Vehicle-to-X applications

Christoph Gehbauer*, Douglas R. Black, Peter Grant

Energy Storage and Distributed Resources Division, Lawrence Berkeley National Laboratory (LBNL), 1 Cyclotron Road, Berkeley, CA 94720, USA

ARTICLE INFO

Keywords:

Plug-in electric vehicles
Fleet vehicles
Model predictive control
Battery degradation
Vehicle-to-grid
Microgrid

ABSTRACT

The demand for local power resilience is promoting the installation of renewable-based microgrids. Plug-in electric vehicles (PEVs) are rapidly increasing and can play a critical role in microgrid service provision. The capability of bi-directional charging and discharging will transition PEVs from a simple means of transportation to multi-purpose value generating assets. They can balance the inherently fluctuating generation of renewable energy resources and shape customer's electricity demand, while still providing the core service of transportation. Value stacking through those additional services allows PEV owners to draw from a number of revenue streams to offset investment costs. However, accelerated battery degradation is often cited as concern when using PEV batteries for purposes other than driving, which presents a major barrier for broad market adoption. This study seeks to assess the economics and trade-offs of bi-directional use of PEVs when utilized as fleet vehicles. In particular, the usage patterns and benefits for PEV fleet deployment at three U.S. military bases is presented. The results show operational cost benefits for bi-directional application of up to 60.8 % annual return on investment without managing battery health, and up to 106.0 % when actively managing battery health through advanced control strategies. The one year payback period far exceeds the expected installation lifespan of at least ten years. Given the results, utilizing PEV fleets for additional services at U.S. military bases can largely offset the additional cost of bi-directional charging hardware and software compared to standard uni-directional equipment.

1. Introduction

Climate change is leading to more frequent and more intense extreme weather events [1]. Microgrids of renewable distributed energy resources (DERs), such as solar and wind power, paired with batteries or other storage, can both slow climate change and provide backup power in the event of grid outages related to climate change induced extreme weather, other disasters such as earthquakes, or intentional acts. Currently, backup power is most often provided by fossil-fuel powered generators that are only used in emergencies and sit idle the vast majority of the time. Renewable based DERs and microgrids can be used continuously, reducing carbon emissions from electric generation and also provide electric power resilience in the event of grid outages. Energy storage in microgrids is most often provided by stationary Lithium-ion batteries, but plug-in electric vehicles (PEVs) with bi-directional charging and discharging capabilities can serve the same function. PEVs can be considered a lower cost option than stationary batteries because they are procured to provide mobility, but with bi-directional capability can be a substantial energy storage resource. The U. S. Army has recognized the challenges of climate change and the

importance of energy resilience for its facilities by committing to install microgrids and convert to an all electric non-tactical vehicle fleet by 2035 [2].

As the market for PEVs increases, interest in controlling their drivetrain batteries to provide vehicle-to-building (V2B) services such as load shifting and vehicle-to-grid services (V2G) such as frequency regulation increases [3–6]. In addition to helping stabilize the grid, V2B and V2G services, collectively referred to as V2X, can provide economic benefit to PEV owners through either shifting their electricity consumption to lower cost times of day or other utility compensation. Frequency regulation is considered an especially promising application for PEVs as (a) PEVs with bi-directional chargers are able to provide the service, (b) it requires low energy commitments, and (c) grid operators often offer reasonable payments for the energy stored in reserve [7]. Peak-load shaving and load shifting is also an attractive option, as many utility rates utilize either time-of-use (TOU) rates with high prices during an evening peak period or peak demand charges. PEV batteries with bi-directional charging capabilities allow buildings to draw power from the PEV battery instead of the grid, reducing electricity consumed

* Corresponding author.

E-mail address: cgehbauer@lbl.gov (C. Gehbauer).

<https://doi.org/10.1016/j.apenergy.2023.121296>

Received 29 December 2022; Received in revised form 11 February 2023; Accepted 13 May 2023

Available online 27 May 2023

0306-2619/© 2023 The Authors. Published by Elsevier Ltd. This is an open access article under the CC BY license (<http://creativecommons.org/licenses/by/4.0/>).

Abbreviations

AC	Alternating Current
BMS	Battery Management System
C-rate	Charging Rate
CAISO	California Independent System Operator
DC	Direct Current
DER	Distributed Energy Resources
DER-CAM	Distributed Energy Resources-Customer Adoption Model
DOD	Depth of Discharge
DOPER	Distributed Optimal Energy Resources
EOL	End of Life
FMI	Functional Mock-up Interface
GHG	Greenhouse Gas
LBNL	Lawrence Berkeley National Laboratory
LFP	Lithium Iron Phosphate
MPC	Model Predictive Control
NCA	Nickel Cobalt Aluminum
NMC-LMO	Nickel Manganese Cobalt Oxide-Lithium Manganese Oxide
OASIS	Open Access Same-time Information System
PEV	Plug-in Electric Vehicle
PV	Photovoltaic
RC	Resistance-Capacity
ROI	Return on Investment
SOC	State of Charge
SOH	State of Health
SynAS	Synthetic Ancillary Service Generator
TOU	Time of Use
V2B	Vehicle to Building
V2G	Vehicle to Grid
V2X	Vehicle to Building and Grid

from the grid and mitigating the costs incurred under TOU or peak demand pricing structures.

Controls for PEVs providing frequency regulation and load shaping must balance the grid service goals with the PEV owner's sometimes uncertain mobility needs while minimizing the cost of operating the vehicle. Prior research projects have averaged the behavior from groups of thousands of PEVs [6] or used perfect forecasts [8] when identifying the optimal charging and discharging frequency regulation schedule. These approaches work for large installations and for evaluation studies using historical data, but not for new installations or installations with few electric vehicles as limited data is available for characterizing common driving behaviors. Other projects have addressed the uncertainty in inputs using various methods including stochastic dynamic programming [3], stochastic [9,10], robust [5], or fuzzy optimization algorithms [4]. Those models focused on available price data, typically in the Pennsylvania-New Jersey-Maryland Interconnection market, and are not applicable to cases with specific participation rules which can vary considerably across markets. Other recent studies used mixed-integer linear programming [11], hierarchical scheduling [12], a centralized secondary controller to minimize the impacts on battery degradation [13], and a neural-network based on historical data to predict a charging demand schedule combined with a heuristic algorithm to minimize operating cost while ensuring the PEV batteries were fully charged when needed for mobility [14]. All four demonstrated control improvements. However, they focused on frequency regulation only. Another study [12] developed a controller for distributed, individual PEVs but did not enable deeper benefits from coordinating a local fleet.

While V2X services can provide economic benefit to PEV owners, the risk of accelerated electric vehicle battery degradation caused by increased cycling is commonly cited as a concern. At this time little quantitative evidence exists to refute or substantiate these concerns for different grid services. For V2X services to be viable the economic benefit to PEV owners must be higher than the economic cost of providing the services. Degradation of PEV Lithium-ion batteries used exclusively for transportation is well understood. Hereby PEV batteries experience two forms of aging, calendar and cycle aging. Calendar aging refers to battery degradation over time which is mainly driven by cell age and temperature. Cycle aging refers to battery degradation caused by the charging and discharging processes. Prior research studies have shown that calendar aging is caused by solid-state inter-phase formation at the negative electrode [15,16] which causes irreversible capacity loss. Cycle aging is primarily driven by the charging rate (C-rate) of the battery, temperature of the battery, and total withdrawn energy. C-rate is a representation of charging current normalized to battery capacity. A 1C C-rate would charge a fully empty battery in one hour, 2C would charge a fully empty battery in 30 min, and 0.5C would charge a fully empty battery in two hours. Recent studies have shown that total withdrawn energy more accurately captures degradation effects than cycle number with different depth of discharge (DOD) profiles [17]. Due to the effect of different state of charges (SOC), a 20% cycle from 100% to 80% will cause different degradation than a cycle from 40% to 20%. On the other hand, PEV battery degradation when providing V2X services is not as well understood. Prior simulation studies have compared the economic benefit of using V2X for peak load shaving, frequency regulation, and net load shaping to the economic cost of increased battery degradation [18], sometimes with aging mitigation algorithms [19]. The studies showed negligible increases in battery degradation cost when performing peak load shaving and frequency regulation, but that degradation increases can be substantial when providing load shaping services everyday. While one study [18] provided a general understanding of V2X impacts on PEV battery degradation, it did so while assuming that V2X services were either provided identically each day or provided on only 20 days of the year.

Repurposing PEV batteries at the end of their useful life for transportation, commonly referred to as "second-life", can have significant impacts on reducing greenhouse gas (GHG) emissions, and provide a new income stream for PEV owners. To create a second-life battery, the good cells from a used PEV battery are repackaged and used as a stationary battery to provide V2X services. The refurbished battery is expected to be lower cost than a new battery, improving the cost-effectiveness of V2X services, and will provide another revenue stream for PEV owners who are able to sell their used batteries at the end of useful life.

Prior studies have shown that advanced controls that take into account the economic cost of battery degradation improve the viability of V2X services [19]. Model predictive control (MPC) is an option that utilizes weather and load forecasts, known data of PEV battery state, mathematical models of the system, and an optimization algorithm to identify the optimal control strategy for a control horizon of typically 24 h. The models enable estimation of the financial benefits and costs of providing V2X services each day, and the MPC determines the best strategy to minimize total operating cost. Lawrence Berkeley National Laboratory (LBNL) has previously created a hierarchical control system that enables V2X services across aggregated fleets of PEVs [20]. The controller consists of: (a) a fleet scheduling tool gathering input data from the user's predicted trip details, (b) day-ahead and hour-ahead charging and discharging schedules from LBNL's Distributed Energy Resources-Customer Adoption Model (DER-CAM) [21,22], and (c) a real-time controller computing charging instructions [23].

Prior work has utilized MPC for sensitivity studies and deployment of V2G services at the Los Angeles Air Force Base [20,24] while providing PEV usability by maintaining high SOCs of the batteries. The MPC used in these two studies minimized the total cost of operating

the vehicles by varying (a) the charge and discharge power for each time interval in the forecast horizon, (b) the hourly up and down regulation capacity the fleet provides, and (c) the spread of regulation services across the PEV fleet. The MPC was driven by a fleet model tracking the PEV energy storage dynamics, limitations of the physical infrastructure, and the market participation limits. The sensitivity study showed that the economic impacts of V2G services is highly dependent on the vehicle driving patterns, the frequency regulation strategy, and the frequency regulation pricing strategy [20]. Since that work did not have access to real PEV driving data the authors used randomized trip schedules. Performing similar work with real driving data would provide real-world context to their work.

This paper extends prior work by (a) adding a battery degradation model to the MPC to actively manage battery health, (b) evaluating the MPC control approach across several uni- and bi-directional system capabilities, and (c) quantifying the performance of the MPC when applied to PEV fleets using real data. The data used in the simulation study represents monitored load and photovoltaic (PV) production for three military bases in California, and PEV fleet usage data from one base. This paper demonstrates that MPC controls with battery degradation models can provide economic value and satisfactory PEV user experiences.

2. Methodology

This study seeks to quantify the financial benefit of PEVs providing V2X services utilizing advanced control strategies. In particular, a novel approach to consider battery degradation was explored, where an advanced control system actively manages the incurred battery degradation. This section outlines the controller development and evaluation setup.

2.1. Controller development

To date, most PEVs charging is either not controlled, i.e., fully charge the battery as soon as the PEV is plugged-in, or follows simple heuristics, e.g., charge to 80% SOC upon plug-in and then fully charge to 100% SOC before 6:00. Various approaches for advanced control of PEVs for different purposes have been studied, but battery degradation is usually either not accounted for at all, or estimated through post-processing, i.e., reactive or lagging indication. This study, on the other hand, adds battery degradation as part of the overall control objective to predict and actively manage it.

The controller used in this study is based on the Distributed Optimal and Predictive Energy Resources¹ (DOPER) development. DOPER is an open-source controller utilizing the MPC technique for real-world control applications. It was introduced in [25] where it was used to manage PV and behind-the-meter battery storage to reduce customer electricity cost. Since then it has been further developed and is currently evaluated for control of smart buildings, microgrids, and fleet electric vehicles. The implementation of PEVs in DOPER uses methods in [20] with expansion towards reliable regulation bidding and fast execution for real-world application. DOPER also provides the capability of variable timestep optimization which is essential when generating battery dispatches for many PEVs in real-time. In particular, DOPER typically computes the battery dispatch every 5 min. Assuming a 24-h horizon and a constant timestep, the optimization would have to solve 288 timesteps within a 5 min window. This can be challenging, especially for larger PEV fleets. DOPER on the other hand allows for a variable timestep, and therefore only requires solving 25 timesteps, i.e., 24 hourly forecasts and the first 5-min timestep. Since the MPC optimization typically scales exponentially, the 91% reduction in timesteps can enable a multi-fold scale-up.

For this study, DOPER is further expanded with an implementation of a battery degradation model and mechanisms to internally track and forecast battery degradation.

The DOPER controller performs the following steps which are further described in the subsequent sections:

- Update states: Collect the latest PEV battery SOCs and temperatures from the simulation and update the optimization parameters accordingly, see Section 2.2.
- Forecast: Collect the latest forecasts for load, PV, and weather in a 5 min timestep for the optimization horizon of 24 h, see Section 2.2.1.
- Fit degradation model: Use the latest statistics of average power usage, average temperature, and age over the current lifetime of each PEV battery to fit individual linearized battery degradation models, see Section 2.1.2
- Regulation bidding: When the V2X control option is enabled then resample the forecast data to hourly timesteps, filter only PEVs which are scheduled to be available the whole day, and perform optimization to determine regulation bids. Pass regulation bids to the simulation.
- Optimization: Conduct the optimization given latest state and forecast data to establish the optimal dispatch for the next 24 h in a 5 min timestep. When the V2X control option is enabled then add placed frequency regulation bids to constraints.
- Update degradation model: Extract and store incremental statistics on PEV battery average power usage, average temperature, and age, see Section 2.1.2
- Send setpoint: Extract PEV charger setpoints from the results and pass to the simulation, see Section 2.2.

2.1.1. Battery degradation model

There are several different models describing calendar and cycle aging characteristics of batteries, as shown in Table 1. Model formulation varies depending on the chemistry of the underlying battery aging data and whether both calendar and cycling aging are incorporated or modeled separately. The models available in literature address three battery chemistries named for their cathode material — Nickel Cobalt Aluminum (NCA), Lithium Iron Phosphate (LFP), and Nickel Manganese Cobalt Oxide-Lithium Manganese Oxide (NMC-LMO). The three most developed of these models are the NREL [26], Wang [16], and MOBICUS [27] models.

The NREL model includes the most factors related to the coupled effects of calendar and cycle aging for two chemistries and is based on aging data primarily from geosynchronous orbit satellite life qualification tests which have different usage requirements and may not be indicative of aging in PEV use cases. The Wang model was parameterized for the NMC-LMO chemistry, but does not employ actual storage data for calendar aging as it was assumed that low C-rate, low DoD cycling data would be comparable to storage conditions. The MOBICUS project has access to the most robust aging data set from the greatest variety of battery chemistries. However, the overall modeling approach to couple calendar and cycle aging is not clear as only separate calendar and cycle aging models have been published to date.

The Wang model provides the best battery degradation model for use in this study because it is specific to the vehicle type used in this study, i.e., Nissan LEAF, with the NMC-LMO battery chemistry. Furthermore, there is precedence for use of the Wang model, as it was employed in a previous cost-benefit analysis of PEVs providing grid services in [31]. However, there are known limitations with employing the Wang model for economic evaluations of battery degradation:

- Cell-to-Pack Translation: The Wang model was developed with measurements made with small cylindrical 18,650 cells (18 mm diameter and 65 mm tall) with 1.5 Ah and NMC-LMO chemistry produced by Sanyo. Nissan LEAF battery cells are the same chemistry, but have greater capacity at 32.5 Ah and are produced

¹ <https://github.com/LBNL-ETA/DOPER>

Table 1
Semi-empirical battery degradation models and dependencies.

	Calendar aging			Cycle aging				Chemistry		
	Temp	SOC	Time	Temp	SOC	C-rate	DoD	NCA	LFP	NMC-LMO
NREL [26]	✓	✓	✓	✓	✓	✓	✓	✓	✓	
Hoke [28]	✓	✓	✓	✓	✓	✓	✓	✓		
Neubauer [29]	✓	✓	✓	✓	✓	✓	✓	✓		
J. Wang [16]	✓		✓	✓		✓	50%			✓
J. Wang [30]				✓		✓	✓		✓	
D. Wang [31]	✓		✓	✓		✓	50%			✓
MOBICUS [27][32]	✓	✓	✓	✓	✓	✓	✓	✓	✓	✓
Delaille [33]	✓	✓	✓						✓	
Gyan [34]				✓	✓	✓	✓			✓
Petit [35]	✓	✓	✓	✓		✓		✓	✓	
Shuangqi [36]						✓	✓			

by AESC. While there is some evidence that similar chemistries will exhibit similar general degradation profiles, the extent of the impact of varying degradation behavior between different manufacturers of the same chemistry cells remains unknown [27]. It is known, however, that cell-to-pack translation gives biased results as battery packs experience additional degradation beyond what is expected at the cell level. This is likely due to non-uniform temperature distributions due to pack imbalances which go undetected in the Battery Management System (BMS) [37]. To prevent non-uniformity, this study uses a homogeneous battery temperature model where temperatures are evenly distributed across the battery pack. With this method, it can be reasonably assumed that all cells experience similar temperatures due to charge or discharge and therefore are aging similarly.

- Time Resolution: Current battery aging models do not take micro-cycling into account and calculate temperature related degradation using hourly averaged temperatures. Therefore, they cannot fully capture the effects of small perturbations in cell temperature and SOC that frequency regulation will likely entail. This study uses high-fidelity simulation with sub-second sampling to accurately capture battery temperature and compute degradation.
- Data Limitation: Battery aging and operation is unclear beyond 30% capacity fade and beyond 10 years time as no empirical dataset has been generated. Furthermore, operation at extreme temperatures (below 0 °C and above 40 °C) is less clear. However, as battery asset End of Life (EOL) is defined at 30% capacity fade and all batteries are operated within normal operating temperatures, this is not a limiting factor in this study.

Wang et al. [16] describes calendar aging to be driven by time and temperature, as shown in Eq. (1).

$$Q_{Calendar} = A * \exp(-E_a/RT) * t^{0.5} \quad (1)$$

The lost capacity from calendar aging, $Q_{Calendar}$ in percent, is calculated with a pre-exponential factor, A defined as $14,876 \text{ day}^{-0.5}$, and the exponent of the required activation energy, E_a as 24.5 kJ/mol , the universal gas constant, R as 8.31 J/(K * mol) , the average temperature of the battery cell, T in Kelvin, and the total lifetime of the battery cell, t in days.

Cycle aging is described in Eq. (2).

$$Q_{Cycle} = (a * T^2 + b * T + c) * \exp[(d * T + e) * C_{rate}] * Ah_{throughput} \quad (2)$$

The lost capacity from cycle aging, Q_{Cycle} in percent, is calculated with the average temperature of the battery cell, T in Kelvin, the average C-rate, C_{rate} in C, the average energy throughput, $Ah_{throughput}$ in Ah, and a set of fitted coefficients. The coefficients are: $a = 8.61E-6 \text{ (Ah*K}^2\text{)}^{-1}$, $b = -5.13E-3 \text{ (Ah*K)}^{-1}$, $c = 7.63E-1 \text{ Ah}^{-1}$, $d = -6.73E-3 \text{ (K*C)}^{-1}$ and $e = 2.35 \text{ C}^{-1}$.

2.1.2. Reduced order battery degradation model

In order to implement the non-linear Wang model into the mixed-integer linear programming model of DOPER, several steps are taken to partially linearize the model and, externally to DOPER, track battery statistics needed for the Wang model, such as average temperature and average energy throughput. The Wang model is implemented in an external Python function that is run before the actual optimization in DOPER. This function can quickly compute the incremental battery degradation for the incremental age of the battery, throughout the optimization horizon, and a range of incremental average battery temperatures, e.g., ± 1 Kelvin of the average battery cell temperature. The range of inputs and resulting calendar and cycle aging are then passed to an optimization algorithm to fit a linear regression defined in Eqs. (3) and (4).

$$Q_{Calendar} = \sum_{ts=1}^n a(ts) + b(ts) * T(ts) \quad (3)$$

$$Q_{Cycle} = \sum_{ts=1}^n c(ts) + d(ts) * C_{rate}(ts) + e(ts) * Ah_{throughput}(ts) \quad (4)$$

The fitted coefficients a , b , c , d , and e are all time dependent, where ts refers to the current timestep, to capture the dynamic aging through time. The average battery temperature, T in °C, is calculated based on the initial average temperature and a reduced order resistance-capacity (RC) thermal model internal to the MPC to compute instant battery temperature based on power flow and environment temperature. The RC parameters were empirically derived from field test data, as described in Section 2.2.1, and used in both the controller and simulation model for evaluation. At each iteration of DOPER, the coefficients are recomputed with the updated battery statistics for age, average temperature, and average C-rate over the lifetime, to closely match the non-linear Wang model. However, mismatch between the full Wang model, which is implemented in the simulation model for evaluation, and the reduced order model remains. Fig. 1 illustrates the sensitivity of the Wang model to average battery temperature, the main driver in this study, and the model mismatch of the reduced order model at different points.

Depending on the ambient air temperature and degree of utilization of the battery, the average temperature of the battery cells can vary greatly. While a lightly utilized battery with an average temperature of 15 °C, shown in blue, might result in long life of up to seven years before degrading beyond the 30% EOL criteria, moderate utilization for V2X services can raise the average temperature. At an average of 30 °C, shown in orange, the battery lifetime is reduced to five years. At an average temperature of 45 °C, shown in green, and representative of hot environments with heavy battery utilization, the battery lifetime is significantly shortened to approximately 1.5 years before reaching the 30% EOL criteria. A reduced order model was created to linearize

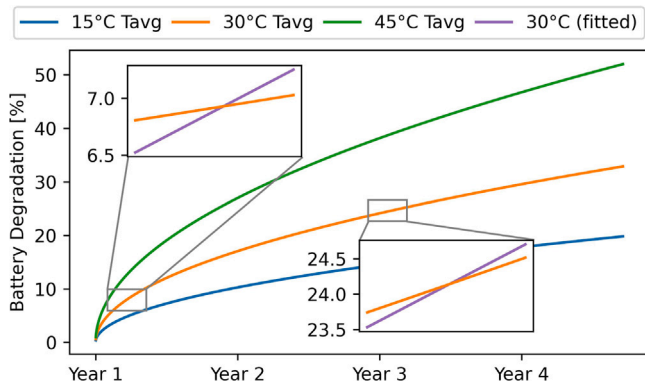


Fig. 1. Illustration of battery degradation ranges and reduced order model mismatch.

the non-linear Wang model for defined small temperature ranges and is represented as purple line in Fig. 1. The sharper the change of degradation as a function of temperature, i.e., at the beginning of the battery life, the higher the model mismatch between the Wang model and the linearized reduced order model. However, while actual battery degradation values might deviate from the full Wang model, the slope of impact matches the direction of the Wang model. This is an important factor as it guides the optimization solver towards a conservative rather than exploitative control policy.

2.1.3. Battery degradation cost function

To implement the economic impact of battery degradation, a battery cost transfer function is used. The battery degradation cost, $c_{\text{degradation}}$ in \$, is hereby defined by the sum of incremental calendar and cycle degradation, defined in Eqs. (3) and (4), multiplied by the battery replacement cost, c_{bat} in \$ and normalized by the end of life criteria, as shown in Eq. (5).

$$c_{\text{degradation}} = (\Delta Q_{\text{Calendar}} + \Delta Q_{\text{Cycle}}) * c_{\text{bat}} / \text{EOL} \quad (5)$$

In this study, the usable battery capacity is hereby defined by an EOL of 30% capacity loss. A second EOL condition exists when internal resistance rise reaches 100% of the original resistance which limits the instant power delivery. Multi-year test data for Nissan LEAFs produced by Idaho National Laboratory indicated that no resistance EOL condition was encountered before the capacity EOL criteria was reached [38–41] [42]. Therefore, it is assumed that resistance increase is not a limiting factor for this study and only the capacity EOL condition is considered for computing the degradation cost.

The objective of DOPER is expanded to include the cost of battery degradation, shown in Eq. (6).

$$\min c_{\text{energy}} + c_{\text{demand}} - r_{\text{frequency}} + c_{\text{degradation}} \quad (6)$$

The original objective to minimize total electricity cost, that is cost for energy and demand, c_{energy} and c_{demand} respectively, and reward from frequency regulation, $r_{\text{frequency}}$, is expanded with the total cost for battery degradation, $c_{\text{degradation}}$, introduced in Eq. (5).

The implementation of frequency regulation within DOPER is expanded to include individual battery utilization. The original implementation in [20] accounted for a net power flow at the battery of zero Watts when symmetric bids were placed. Given Eqs. (3) and (4), a net power flow of zero Watts does not have an effect on battery degradation, hence frequency regulation would not lead to any battery degradation in the controller. To include battery degradation when providing frequency regulation, the MPC model is expanded to include inter-timestep power flows where the average of the absolute regulation up and down bids for each timestep, in case of symmetric bids the full regulation up or down bid, is accounted as battery power flow. Since this represents a worst-case scenario where the battery is constantly

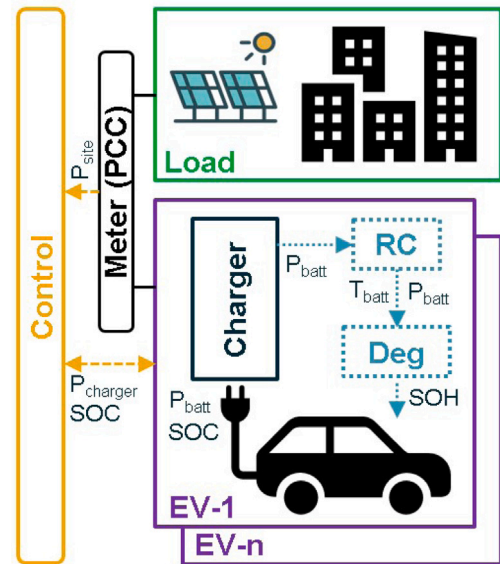


Fig. 2. Coupling of controller with high-fidelity co-simulation.

cycled with full power over the full hour, a duty-cycle factor is added to moderate the battery power flow. Analyzing the data from the LAAFB field demonstration, see Section 2.2.2, typical duty-cycles varied between 40% and 70%. In this study the duty-cycle of the controller and simulation were matched to the average of 54.8% from the recorded data.

2.2. Evaluation

This study evaluates the capability of various advanced control strategies to assess the financial benefit of PEVs. While simple rule-based control algorithms can be simulated offline, i.e., pre-computed control setpoints are passed as input to a simulation, advanced control algorithms such as MPC require feedback from the resources being controlled as well as time-synchronized weather and load forecasts. It is, therefore, crucial to evaluate advanced control algorithms through online simulations, also known as co-simulation, where at each simulation timestep information is exchanged with the controller, and new setpoints are passed to the simulation model. While various ad-hoc approaches to couple controllers with simulation models exist, this study leverages the Functional Mock-up Interface² (FMI) standard which is widely adopted by industry including large companies such as Bosch and Siemens [43]. The simulation model is developed in the modeling language Modelica³ and exported as a stand-alone simulation model using the FMI standard. A Python script, PyFMI,⁴ binds the DOPER controller and simulation model. Fig. 2 illustrates the functionality of the co-simulation and data flow.

The simulation model is developed to realistically represent a fleet of PEVs, illustrated as purple boxes. The PEV drivetrain battery is modeled using the high-fidelity electrical model of a stationary battery from the Modelica Buildings Library⁵ (MBL), illustrated as electric vehicle in the purple box, and expanded to use real driving profiles obtained from the LAAFB fleet management data and external input of battery health. An PEV charger model, black outline in the purple box, is implemented by expanding the MBL implementation with external

² <https://fmi-standard.org/>

³ <https://modelica.org/>

⁴ <https://github.com/modelon-community/PyFMI>

⁵ <https://github.com/lbl-srg/modelica-buildings>

inputs for alternating current (AC) power setpoint control and the functionality to disconnect from the power grid, i.e., un-plug the PEV. The charger model takes an AC power setpoint as input and returns the resulting AC power flow, P_{charger} , and PEV battery SOC, subject to available capacity of the PEV battery and conversion losses, see Table 2. Additional models are added to simulate the battery health based on the Wang battery degradation and RC thermal models. The RC model is derived from empirically collected data, see Section 2.2.1, and computes PEV battery pack temperature, T_{batt} , based on the battery direct current (DC) power flow, P_{batt} , and ambient air temperature supplied by external data. The Wang degradation model takes the battery DC power flow and pack temperature as input to compute the state of health, SOH, of the battery. The SOH is used as a scaling factor between 0 to 100% and applied to the battery capacity parameter. The PEV drivetrain battery exchanges SOC and electric power flow information with the charging station. The PEV, charger, and battery health models, i.e., all models in purple outline, are instantiated with a new set of parameters for each PEV within the fleet. The load models, green outline, use the external load and PV profiles from the respective military bases to provide a net-load profile. The utility meter, black outline, combines the individual PEVs and load power flows to the site AC power flow, P_{site} . The controller, yellow outline, receives the site power flow information and each charging station's AC power flow and SOC information, if an PEV connected. The controller then computes the charging station AC power setpoints for each available PEV. While the evaluation of the controller is set to a 5 min interval, the simulation models are continuously evaluated with the CVODE⁶ variable timestep solver and a minimal timestep of 1 ms. The continuous evaluation is important to accurately represent and capture simulation state events, for example when a PEV battery is fully empty or full the battery power drops to zero instantly instead of awaiting the next fixed timestep evaluation. The PEV simulation model and the aggregated fleet model are publicly available through the Smart Control of Distributed Energy Resources⁷ (SCoDER) package [25].

2.2.1. Input data

All input data for the evaluation of the different scenarios is summarized in Table 2 and further described in this section.

To test the variability in performance this study uses datasets from three U.S. military bases:

- **Los Angeles Air Force Base (LAAFB)** is a United States Air Force base and the headquarters for the Space and Missile Systems Center. Located in El Segundo, California, LAAFB is responsible for research and development of space-based military systems as well as equipment acquisition. There are currently 1300 active duty military members at LAAFB, as well as 1700 civilian workers. The available data includes (a) base load data from April 1, 2016 to November 8, 2018, (b) PEV trip data from January 1, 2016 to September 6, 2018, and (c) PV data from January 1, 2016 to May 1, 2019. The base load and PV data both have 5-min sampling frequencies.
- **Parks Reserve Forces Training Area (PRFTA)** serves both the Army Reserve and the Joint Force. Located in Dublin, California, this base supports military readiness by educating service members, performing military intelligence operations, and providing battlefield simulation opportunities. The available data set for PRFTA includes base load data with a 15 min sampling frequency spanning 2019 and 2020. PRFTA does not have PV or PEV fleet data.

- **Fort Hunter Liggett (FHL)** is considered a top training center for the U.S. military. This 65,000 acre facility is often used for large-scale joint exercises using both on base and nearby PRFTA sub-installations. FHL has a permanent population of only 265 civilians and military residents, but houses up to 40,000 people during large training exercises. The base load dataset for FHL contains data from October 2017 through September 2019 with a 15 min sampling frequency. The PV data spans 2011 to 2020.

The datasets were in different formats, from different times, and used different sampling frequencies. Combining the data sets required pre-processing to ensure compatibility. Since the LAAFB dataset already satisfied the requirements for simulation, all other datasets were reformatted to match. In particular, data was filtered for missing or outlier data, resampled to 5 min intervals, and shifted to align with the weekdays in the LAAFB dataset for the year 2017. To resolve erroneous data, all points more than three standard deviations below the mean in a rolling 30 day window were replaced with interpolated values between the prior and following points. PRFTA had a prolonged data gap from July 22 to July 31 which was filled with data from the previous week. All bases with PV generation had large data gaps in PV generation. PV and load was disaggregated using simulated PV generation based on historic weather data obtained through DarkSky⁸ and PV nameplate capacity. Historic weather data for the periods of the datasets was used to model environmental conditions. LAAFB shows the highest electric load, with a mean of 2696 kW and a maximum of 5760 kW. PRFTA shows the lowest load, with a mean of 989 kW and a maximum of 1854 kW. FHL shows a moderate load, with a mean of 1026 kW and a maximum of 2993 kW.

Datasets for fleet trip data was obtained from the respective fleet management entity for the LAAFB base. The fleet management at military bases usually require day-ahead scheduling of fleet vehicles which results in little uncertainty about PEV availability for V2X services. For this study it was assumed that the modeled fleet matches the LAAFB fleet of 12 Nissan LEAFs model 2012. The dataset includes 1247 trips with reservation start and end times and the miles driven. The availability of a vehicle is defined as the time that it is not out on a trip compared to the total duration of the data set. The average availability across the fleet was 92.0%. Trip energy consumption was estimated using the 30 kWh/mile rated efficiency of a 2012 Nissan LEAF. Fig. 3 shows the actual fleet of Nissan LEAFs at the LAAFB, where each PEV is connected to a 15 kW bi-directional charging station.

Data pre-processing options for the PEV fleet data are grouped in the following scenarios:

1. **Original:** The original option uses the PEV fleet data as it occurs in the dataset. This scenario uses the same number of PEVs as are installed in the field, and assigns the driving trips to the PEVs as observed in the dataset.
2. **Optimized Fleet:** The optimized fleet option identifies the minimum number of PEVs needed to meet the observed driving demands, simulates a fleet with that number of vehicles, and reassigns driving trips based on availability and total miles driven. A minimum plug-in time between trips of 30 min is used to ensure batteries can be recharged. This parameter was empirically determined and may vary based on specific fleet utilization.
3. **Optimized Fleet, Extras Plugged:** This option uses the same fleet optimization code, but assumes that it uses the existing PEVs in the optimized manner and not through purchasing fewer PEVs. The extra PEVs which are not needed to satisfy trips are assumed to be plugged-in constantly, and essentially serve as stationary batteries.

⁶ <https://computing.llnl.gov/projects/sundials/cvode>

⁷ <https://github.com/LBNL-ETA/SCoDER>

⁸ <https://darksky.net>

Table 2
Overview of evaluation scenarios.

Base load	LAAFB (5.8 MW-peak) or PRFTA (1.9 MW-peak) or FHL (3.0 MW-peak)	
PV	1.8 MW-peak based on LAAFB dataset	
Tariff	SCE TOU-8	
Frequency Regulation	1 or 100 kW minimum bid (54.8% duty cycle)	
Control Scenarios	see Table 3	
Fleet Size	Original (12 PEVs) or Optimized (8 PEVs) based on LAAFB dataset	
Charging Stations	One dedicated per PEV	
PEV Model	Nissan LEAF 2012	Nissan LEAF 2022
PEV Battery Capacity	24 kWh	60 kWh
Charger Power	7.6 kW (uni-dir) or 15 kW (bi-dir)	7.6 kW (uni-dir) or 50 kW (bi-dir)
Second-Life Battery Capacity	None or 144 kWh (Original Fleet) or 96 kWh (Optimized Fleet)	None or 360 kWh (Original Fleet) or 240 kWh (Optimized Fleet)
Second-Life Power	None or 72 kW (Original Fleet) or 48 kW (Optimized Fleet)	None or 180 kW (Original Fleet) or 120 kW (Optimized Fleet)
Second-Life Thermal Parameter	C = 14.6 MJ/K R = 7.5 mK/W	C = 36.4 MJ/K R = 18.7 mK/W
PEV Battery Thermal Parameter	C = 7.28 MJ/K R = 3.74 mK/W (plugged-in) or 1.87 mK/W (driving)	
PEV Efficiency	Charging = 96%, Discharging = 96% (combined charger and PEV efficiencies)	
PEV Battery End of Life	30% loss of capacity	



Fig. 3. Plug-in electric vehicle fleet of Nissan LEAFs at the Los Angeles Air Force Base.

The PEV battery thermal model for both the controller and simulation is derived from empirical test data from the field demonstration at LAAFB. An extensive battery cycling for three of the Nissan LEAFs over the course of a day was performed while monitoring battery pack temperature, battery DC power flow, and ambient air temperature. Note that the 2012 Nissan LEAFs report four battery pack temperatures which are averaged for this analysis. The resulting data is used to fit a first order RC model, i.e., single resistor and single capacitor. The resulting parameters are $R = 3.73$ mK/W and $C = 7.28$ MJ/K. Since data is only available for parked vehicles, it is assumed that the thermal resistance when driving is 1/2 of R , while the thermal mass of the

battery, C , remains constant. The thermal parameters for the second-life battery are scaled based on total energy.

The initial approach of this study was to model the original LAAFB fleet with the deployed model 2012 Nissan LEAFs. In order to project results for newer vehicles, the newest version of the Nissan LEAF model 2022 with an increased battery size from 24 kWh to 60 kWh is also included. The RC parameters for the 2022 Nissan LEAF are the same as the observed ones for the 2012 Nissan LEAF, assuming that battery pack size remains equivalent and capacity increase is solely attributed to cell chemistry improvement. The capabilities of the PEV charging stations are matched to the LAAFB field installation with maximum power of 7.6 kW for uni-directional and 15 and 50 kW, respectively for the 24 and 60 kWh Nissan LEAFs, for the bi-directional charging stations. The number of charging stations is equal to the fleet size. Based on LAAFB field test results, it was determined that the battery replacement cost for the 2012 Nissan LEAF is \$ 6000 (250 \$/kWh) while the battery replacement cost for the 2022 Nissan LEAF was researched online and estimated to be \$ 10,500 (175 \$/kWh). Military facilities typically separate infrastructure investment, e.g., for uni-directional PEV charging infrastructure, from fleet acquisition. The incremental investment cost considered in this study includes the cost for additional controls and software maintenance, estimated to be \$ 5000 per PEV, and the difference between a uni- and bi-directional charging station where applicable, estimated to be \$ 5000 per PEV for a 15 kW charger and \$ 10,000 for a 50 kW one. Depending on the type of charging station this results in a total incremental investment cost of either \$ 5000 or \$ 10,000 per PEV. The cost for the bi-directional charging station is based on the assumption that a consumer grade bi-directional charging station costs about \$ 1500, for example the 12 kW Emporia V2X Charging Station [44], and a consumer grade uni-directional charging station costs about \$ 500, which results in an incremental cost of \$ 1000. Assuming that a commercial uni-directional charger costs around \$ 2000, based on experience of the LBNL team working with field installations at military facilities, the cost is four times higher,

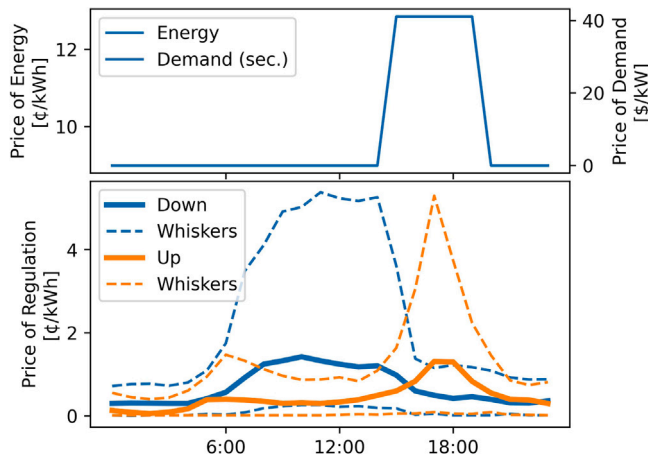


Fig. 4. Overview of time-of-use tariff and hourly regulation prices.

which results in an incremental cost of the bi-directional charging station of \$ 4000. Another \$ 1000 is added for miscellaneous items such as approvals, switch gear, and commissioning, which then results in the described \$ 5000 incremental cost for a 15 kW bi-directional charging station per PEV. The 50 kW bi-directional charging station is assumed to have double the incremental cost, i.e., \$ 10,000 per PEV. The cost for controls and software maintenance are based on LBNL's experience with field installations at military facilities, and includes the assumption that a moderately sized fleet of 20 PEVs would incur \$ 100,000 investment cost, which can be broken down into \$ 20,000 for control design, hardware, and commissioning, and a remaining \$ 80,000 for maintenance, which is assumed to cover 12 months of full time equivalent labor. Over a 10 year life cycle this results in about one month of maintenance per year, or two days per month.

2.2.2. Tariff data

The tariff data used in this study is Southern California Edison's TOU-8 tariff⁹ with option D for the 2 to 50 kV interconnection released on June 1, 2022. It defines two price periods in summer, 16:00 to 21:00 for high-peak and 21:00 to 16:00 for off-peak, and three price periods in winter, 16:00 to 21:00 for high-peak, 8:00 to 16:00 for off-peak, and 21:00 to 8:00 for mid-peak. The prices for energy are 9.0 and 12.8 ¢/kWh in summer for off-peak and high-peak, and are 7.5, 9.5, and 10.6 ¢/kWh in winter for off-peak, mid-peak, and on-peak periods. In addition, the TOU-8 tariff incurs a monthly demand charge for the overall peak of 19.1 \$/kW throughout the year, and an additional 41.1 \$/kW for the high-peak period in summer and 10.4 \$/kW for the high-peak period in winter. Rates on weekends and holidays follow the same time periods, but are slightly lower. The TOU-8 tariff is applied to all simulation scenarios, including those located outside of SCE's territory.

The prices for frequency regulation were obtained from the California Independent System Operator's (CAISO) Open Access Same-time Information System (OASIS) website.¹⁰ Data was analyzed for the full year of 2021 and processed to align weekdays with those from the base load dataset. Fig. 4 illustrates the TOU-8 prices in summer on the upper subplot and prices for frequency regulation on the lower subplot.

The dynamic prices for frequency regulation are shown as hourly plots of median prices, in bold, and associated upper and lower whisker, defined as 25th or 75th quartile plus 1.5 times the inner quartile range of 75th minus 25th quartile, in dashed lines. Regulation down, where on-site resources consume grid electricity, is shown in blue and regulation up, where on-site resources feed-in electricity, is shown in

orange. In this dataset, prices for regulation down are higher during the daytime, while prices for regulation up are higher during the afternoon. This corresponds to the general trend in California where renewable generation, especially from PV, tends to cause over-supply during the daytime, and under-supply during late afternoon peaks, also known as the California "duck-curve" [45]. However, instant regulation requests can largely vary in time and far exceed median prices. The three occurrences of highest prices for regulation up are all in the afternoon, i.e., 2021-09-09 17:00 with 43.8 ¢/kWh, 2021-06-17 18:00 with 42.6 ¢/kWh, and 2021-07-12 18:00 with 42.6 ¢/kWh, while the ones for regulation down are throughout the day, i.e., 2021-01-30 12:00 with 22.1 ¢/kWh, 2021-02-15 08:00 with 20.0 ¢/kWh, and 2021-02-14 13:00 with 16.7 ¢/kWh. In order to participate in the CAISO day-ahead market for frequency regulation, hourly bids of at least 100 kW must be submitted. Depending on the bids and resources, CAISO then seeks to balance utilization based on resource type. In the case of batteries, symmetric bids for regulation up and down are advised, and CAISO seeks to balance the energy demand at net-zero or slightly towards regulation down to account for resource efficiency and keep SOC near the middle of resource-specified minimums and maximums. However, resource utilization can largely vary based on the instant needs of the electric power grid. In [46] the CAISO regulation dispatch for the LAAFB was analyzed, and an open-source Synthetic Ancillary Service Generator (SynAS) package¹¹ to generate synthetic dispatches was introduced. This study uses the SynAS package to simulate the regulation dispatch and its impact on battery health.

2.2.3. Scenarios

This study evaluates a large range of parameters to quantify the benefit of PEVs for various applications. This includes uni-directional charging, V2B, and V2X applications. The evaluation scenarios are listed in Table 3 and include a parametric grid of base load (LAAFB, PRFTA, or FHL), PEV battery size (24 or 60 kWh), minimum bid size for frequency regulation (1 or 100 kW), fleet size (original or optimized), and fleet scale relative to the base load.

A total of 11 control scenarios are explored. The *ChFull* scenario is the reference scenario for this analysis where it fully charges the PEV as soon as it is plugged in. The *Ch80%* scenario utilizes simple logic to immediately charge to 80% SOC when the PEV is plugged in, and then charge the remaining 20% in-time for the next trip, reducing the SOC level when not used. Both cases only provide uni-directional charging without capability to discharge the PEV. The first advanced control case is *uni-dir* where only charging of the PEV is enabled, but scheduled using MPC. The *V2B* and *V2X* cases enable bi-directional charging and provide either building, or building and grid support, if the MPC controller requests it. The *V2B (Stat)* and *V2X (Stat)* cases provide the same functionality, but include two stationary second-life batteries. The second-life batteries are assumed to use the first batch of fleet PEV batteries that reached EOL and were removed from the fleet PEVs. The second-life battery capacity is assumed to have a capacity equal to 50% of the PEV fleet battery capacity. While all of the above cases are associated with the same electric power meter, the cases labeled with (*sep.*) have PEVs located at a separate meter which disaggregates the building load from the PEV fleet. Note that all MPC cases are evaluated with and without the battery degradation model in the controller objective, to quantify the benefit of including such.

3. Results

The results were derived from 720 individual multi-year co-simulations. This section first introduces the high-level summary results with the main findings. It then dives deeper into the mechanics of frequency regulation revenue and bidding, battery degradation, and sensitivity of the results by analyzing one specific scenario (referred to as Example-A) for LAAFB load and PV data, model 2012 Nissan LEAFs, optimized fleet size, and 1 kW minimum regulation bid.

⁹ <https://www.sce.com/business/rates/large-business>

¹⁰ <http://oasis.caiso.com/mrioasis/logon.do>

¹¹ <https://github.com/LBNL-ETA/SynAS>

Table 3
Overview of control scenarios.

	Controller	Charger	Vehicle building support	Vehicle grid support	Visible base load	Second-life stationary storage
ChFull	on/off	uni-dir	False	False	False	False
Ch80%	heuristic	uni-dir	False	False	False	False
uni-dir	mpc	uni-dir	False	False	False	False
V2B	mpc	bi-dir	True	False	True	False
V2B (Stat)	mpc	bi-dir	True	False	True	True
V2X	mpc	bi-dir	True	True	True	False
V2X (Stat)	mpc	bi-dir	True	True	True	True
ChFull (sep.)	on/off	uni-dir	False	False	False	False
Ch80% (sep.)	heuristic	uni-dir	False	False	False	False
uni-dir (sep.)	mpc	uni-dir	False	False	False	False
V2X (sep.)	mpc	bi-dir	False	True	False	False

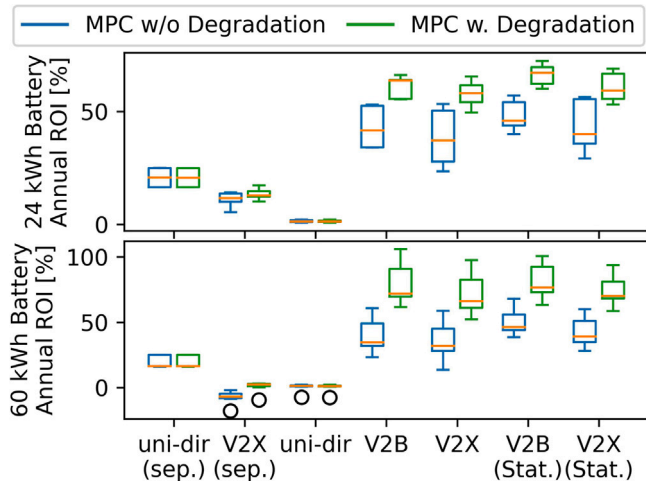


Fig. 5. Annual return on investment rates across control scenarios with and without considering battery degradation.

3.1. Summary results

The benefit of controlled charging and discharging of PEVs to provide services is assessed by computing the annual return on investment (ROI) in percent, defined as annual operational cost savings divided by the total investment cost. Using the ROI metric allows quantifying the benefit of the PEV fleet as an independent service without close ties to the actual load size. Fig. 5 summarizes the results for the different control scenarios.

The results for all parametric simulations, including the three base loads, two fleet sizes, and two minimum regulation bids are grouped into box-whisker plots to illustrate the data trends. The y -axis shows the annual ROI, in %, for both the 24 kWh (top) and 60 kWh (bottom) scenarios. The x -axis lists all seven MPC control scenarios defined in Table 3. Each control scenario includes a set of box-whisker plots for MPC without consideration of battery degradation in the objective, in blue, and MPC with consideration of battery degradation, in green. The first two control scenarios uni-dir (sep.) and V2X (sep.) are presenting scenarios where the PEV fleet is located on separate utility meters and therefore cannot impact the electricity bill of the military base. For both cases no significant benefit to include battery degradation in the control objective is apparent. The uni-dir (sep.) case for the 24 kWh battery size shows annual ROIs between 16.4 and 25.0 (median at 20.7) % while the 60 kWh battery size shows savings between 15.9 and 25.0 (median at 16.5) %. The cases with V2X (sep.), where PEVs can utilize bi-directional charging to either offset demand charges from charging other PEVs or bid into the regulation market, show little variation with a median of 12.8 and 2.3%, respectively for the 24 and 60 kWh battery sizes with degradation. All other control scenarios include a single

utility meter for the military base load and PEV fleet. The uni-dir case allows the MPC controller to control each PEV's charging behavior to avoid increasing monthly demand charges for the military base and to shift charging to lower-priced times. The benefit of MPC for this uni-dir case is negligible, with median ROIs of 1.3%. The V2B control scenario on the other hand, where the fleet PEVs can be used to shift base load demand, yields great benefit for both with and without considering battery degradation. The annual ROIs range between 34.0 and 53.2 (median at 41.6) % and between 23.1 and 60.8 (median at 34.5) % respectively for the 24 and 60 kWh battery size. When considering battery degradation the benefits increase respectively between 55.4 and 66.3 (median at 63.8) % and between 61.7 and 106.0 (median at 71.9) %. The V2X case, where in addition to V2B also V2G is enabled, the annual ROIs without considering battery degradation range between 23.5 and 53.3 (median at 37.2) % and 13.6 and 58.8 (median at 31.9) % respectively for the 24 and 60 kWh battery sizes. The benefit of considering battery degradation increases the ROIs respectively to 49.5 and 65.5 (median at 58.1) % and 52.2 and 97.5 (median at 66.2) %. The last two control scenarios, V2B (Stat.) and V2X (Stat.) add the stationary second-life storage to the available resources. The annual ROIs are moderately higher than in the cases without stationary storage, and the general trend of great incremental benefit when including battery degradation is apparent. The detailed results for the Example-A are given in Table 4.

The Example-A uses the optimize fleet function which reduces the fleet size from the original 12 to 8 PEVs. This results in an investment cost of \$ 40k for the uni-directional cases and \$ 80k for the bi-directional cases. The base case, ChFull, results in a total electricity cost of \$ 3479k and an accumulated battery degradation cost of \$ 7.7k, which results in total operational cost of \$ 3487k per year. The Ch80% and uni-dir cases lead to equivalent cost. Without considering degradation in the controller, the V2B case reduces the electricity cost by \$ 39k but increases the degradation cost by \$ 6k which leads to total operational cost savings of \$ 33k per year or an annual return of 41.1%. The V2X case results in higher electricity cost with \$ 37k reduction from the base case, but regulation revenue of \$ 9k, resulting in savings of \$ 46k which is \$ 7k higher than the V2B case. However, the degradation cost increases to \$ 24k which results in total operational cost savings of \$ 31k per year or an annual return of 38.5%, which is lower than V2B. When considering degradation to actively manage PEV battery health, both the V2B and V2X cases significantly reduce the degradation cost respectively by 22.9 and 36.9%. At the same time electricity cost is also reduced in both cases, leading to increased annual return rates of 55.5 and 56.0% respectively for the V2B and V2X cases.

A summary of the median results for all cases and across all scenarios can be found in the detailed table in Appendix.

3.2. Regulation bidding

The establishment of regulation bids for the day-ahead market is a complex trade-off where available resources, such as the fleet PEVs,

Table 4
Detailed results for Example-A.

	ChFull	Ch80%	uni-dir	V2B	V2X
Total Electricity Cost [k\$/a]	3479.0	3479.0	3478.6	3439.9	3441.7
Regulation Revenue [k\$/a]	0.0	0.0	0.0	0.0	9.3
Total Operational Cost [k\$/a]	3486.7	3486.7	3486.3	3453.8	3456.0
Operational Cost Savings [k\$/a]	0.0	0.1	0.4	32.9	30.8
Investment Cost [k\$]	40.0	40.0	40.0	80.0	80.0
Degradation Cost [k\$/a]	7.7	7.7	7.7	14.0	23.6
Annual Return [%]	0.0	0.2	1.0	41.1	38.5
Total Electricity Cost w Deg. [k\$/a]	n/a	n/a	3478.6	3431.6	3434.2
Regulation Revenue w Deg. [k\$/a]	n/a	n/a	0.0	0.0	7.2
Total Operational Cost w Deg. [k\$/a]	n/a	n/a	3486.3	3442.4	3442.0
Operational Cost Savings w Deg. [k\$/a]	n/a	n/a	0.4	44.4	44.8
Degradation Cost w Deg. [k\$/a]	n/a	n/a	7.7	10.8	14.9
Annual Return w Deg. [%]	n/a	n/a	1.1	55.5	56.0

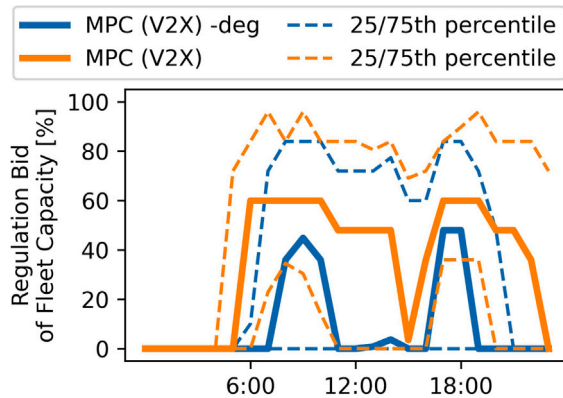


Fig. 6. Frequency regulation bidding pattern for V2X control scenario with and without considering battery degradation in the controller.

need to be balanced between providing V2B and V2G services. The Fig. 6 illustrates this regulation bidding behavior for the Example-A.

The V2X control strategy, where participation in the frequency regulation market is allowed, is shown when the MPC controller includes battery degradation, in blue, and when it does not, in orange. The y-axis shows the symmetric regulation bid as percentage of full fleet capacity. Note that full fleet capacity is defined as the sum of maximal charging or discharging power for each of the PEVs. The plot shows the median, in bold, and 25th and 75th percentiles, as dashed lines. The data is filtered to only include days where at least one hourly bid is submitted. While participation of the V2X scenario without degradation is 56.1% of time, participation decreases to 29.5% of time when considering battery degradation. Both control scenarios show median and percentiles of 0% until 6:00, but with outlier maximum values of up to 100% in rare cases. This can be explained by the MPC controller prioritizing the PEV battery SOC management for the upcoming day over the typically low regulation revenue during this period, as shown in Fig. 4. Starting from 6:00 to 14:00 the scenarios without degradation range between a median of 48 and 60% for most of the time. A significant dip from 15:00 to 16:00 is present which can be attributed to the switch in regulation rewards, shown in Fig. 4, where rewards for regulation down start to decline while rewards for regulation up are still low. The MPC controller therefore prioritizes V2B over V2G to reduce the electricity bill. Regulation bidding reverts to mid-day levels until the late evening hours where it initiates preparation of the PEV batteries for the next day. The control scenario with degradation on the other hand shows bids well below, with median bids only present from 8:00 to 11:00 and 17:00 to 18:00, where they range between 36 and 48%. Bidding at the 75th percentile remains at levels similar to the scenario without degradation.

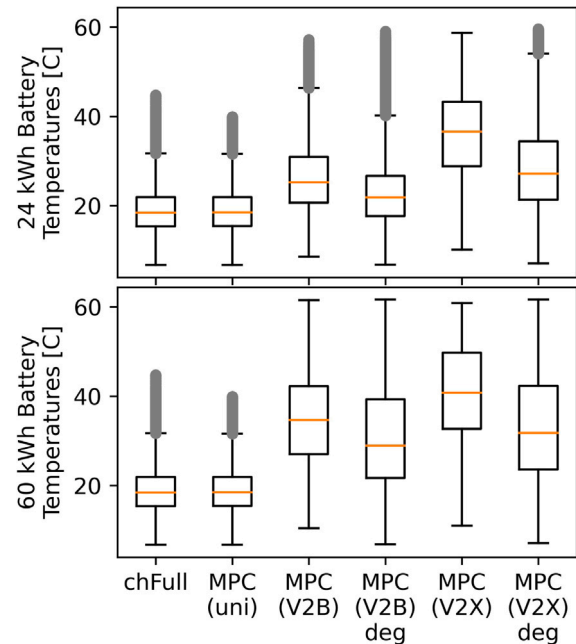


Fig. 7. Distribution of battery temperatures across control scenarios.

3.3. Battery degradation

The quantification of battery degradation is a major focus of this study. The following plots focus on the calendar aging, which mainly depends on the passed time and average battery temperature. Since passed time cannot be influenced, the major variable to control is the average battery temperature. Fig. 7 illustrates the battery temperature distribution across different control scenarios and Fig. 8 illustrates the effect on battery degradation. Both figures are derived from Example-A.

The Fig. 8 is divided into two subplots, the 24 kWh battery size on top and 60 kWh battery size on the bottom. The y-axis shows the battery temperature distribution for all fleet PEVs across the multi-year study. The x-axis shows six selected control scenarios. The ChFull is the base case where PEVs are immediately fully charged when plugged-in. Temperatures range between 6.7 and 44.7 (median at 18.4) °C. The uni-dir scenarios use MPC to perform smart charging, which results in slightly lower temperatures between 6.7 and 39.9 (median at 18.5) °C. All other V2B and V2X cases result in median and average temperatures higher than the base case, regardless whether battery degradation is considered or not. However, control scenarios considering battery degradation show lower median temperatures, e.g., for 24 kWh battery size the MPC (V2B) deg reduces median temperatures by 3.3 °C and MPC (V2X) deg reduces median temperatures by 9.4 °C. Maximum temperatures across all cases are 59.6 °C for 24 kWh and 61.6 °C for 60

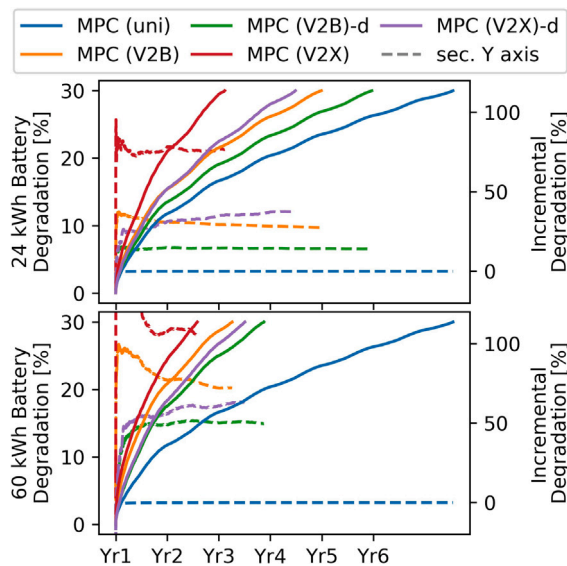


Fig. 8. Battery degradation across multiple control scenarios.

kWh battery sizes which is within the typical operating range of 60 °C for PEV drivetrain batteries. Fig. 8 illustrates the effect of the different control scenarios and battery temperatures on the battery health.

Similar to the previous figure, Fig. 8 is divided into two subplots for 24 and 60 kWh battery sizes. The primary y-axis shows evaluated battery degradation, as solid lines in percent, and the secondary y-axis shows the incremental battery degradation, as dotted lines in percent, in comparison to the base case of fully charging PEVs upon arrival. Note that the simulated battery degradation reflects the true degradation outside the controller, i.e., is obtained from the simulation results and not the controller projections. It is independently computed for each control scenario, regardless if battery degradation was considered or not. The x-axis is the time, in years, of useful PEV battery life. The difference in PEV battery temperatures illustrated in Fig. 7 is reflected in the spread of battery degradation and useful life across the control scenarios. It can be seen that for both battery sizes the uni-dir MPC control scenario results in a useful life of nearly seven years before the battery degradation reaches the 30% EOL threshold, defined in Section 2.2.3. The MPC control scenarios without managing battery degradation, MPC (V2B) and MPC (V2X), result in lowest useful life of 4.0 and 2.1 years respectively for the 24 kWh battery size and 2.3 and 1.6 years for the 60 kWh battery size. The MPC control cases which actively manage battery degradation, MPC (V2B)-d and MPC (V2X)-d, result in moderated useful life of 5.0 and 3.5 years respectively for the 24 kWh battery size and 2.9 and 2.5 years for the 60 kWh battery size. For all control cases the incremental battery degradation remains flat throughout the useful life, indicating that the respective control systems consistently utilize the PEV batteries.

3.4. Sensitivity

As described at the beginning of the Results section the relative size between fleet PEVs and base load impacts the benefit controlled charging and discharging of PEVs to provide. For example larger aggregated energy storage will be able to shift more energy and reduce higher and wider peak load demands than smaller storage, but also require higher investment cost. The following sensitivity study assesses the impact of fleet PEV size relative to base load size. Fig. 9 illustrates this relationship for Example-A.

The figure includes two subplots for two evaluation scenarios. The first one represents control cases without second-life stationary storage and the second one with second-life storage. The y-axis shows the

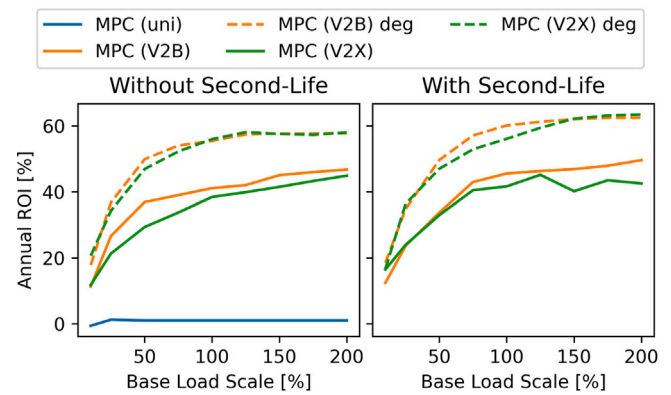


Fig. 9. Sensitivity of annual return rates of load versus PEV fleet sizes across multiple control scenarios.

annual ROI, as defined at the beginning of the Results section. The x-axis shows the base load scale where 100% corresponds to the full base load, i.e., LAAFB load and PV generation. The three control scenarios are MPC with uni-directional control, in blue, MPC with V2B support, in orange, and MPC with V2X support, in green, represent MPC control without consideration of battery degradation. The V2B and V2X cases show results for the inclusion of battery degradation in the objective, shown with dashed lines in the respective colors. It can be seen that for both, with and without stationary storage, the ROIs follow exponential functions starting from about 20% ROI at 10% base load and plateauing around 60% ROI between 100 to 200% base load, for V2B and V2X when considering battery degradation. The uni-directional case on the other hand remains flat at nearly 0% ROI.

4. Discussion

This study seeks to assess the benefit of advanced control strategies for PEV applications. This includes the active management of PEV drivetrain battery degradation, uni-directional smart charging, and bi-directional strategies including V2B and V2G. The input data for this study was obtained from a field demonstration at LAAFB and from other military facilities. The demonstration at LAAFB started in 2015 with a fleet of model 2012 Nissan LEAFs. Given the fast moving pace of new drivetrain battery development, this study used both, the original model 2012 and currently available model 2022 Nissan LEAFs. Obtained data from the 2012 Nissan LEAFs was used to project performance of a model 2022, e.g., the empirically developed battery thermal and degradation models for the 2012 model were applied to the 2022 model.

Battery degradation is complex to assess and causes of such are difficult to evaluate in non-laboratory environments. The implemented Wang battery degradation model was originally developed using small cylindrical battery cells with the same NMC-LMO chemistry as 2012 Nissan LEAFs. This empirical model cycled cells with high C-rates between 0.5 and 6.5 C to establish the model. All those C-rates were well above the ones experienced in this study, e.g., typical C-rates were up to 0.01 C for uni-directional and 0.14 C for bi-directional scenarios. Due to the limited applicability of the Wang model for low C-rates, the cycle aging portion of the Wang model was disabled for both the simulation and controller implementation. With only the calendar aging remaining, the core drivers of battery degradation in this study were the battery age and battery temperature, which in turn was modeled using the empirically developed RC thermal model. While the simulation model used the exact implementation of the Wang calendar aging model, the controller used a linearized model which lead to model mismatch. This mismatch might reduce effectiveness of the explored DOPER controller, but given the significant benefit of inclusion of such shown in the results, the proposed method proved viable.

Table 5
Summary table of median results across all scenarios.

Control scenario	Vehicle battery size [kWh]	Total elec. cost [k\$/a]	Reg. rev. [k\$/a]	Total oper. cost [k\$/a]	Oper. cost savings [k\$/a]	Invest. cost [k\$]	Annual return [%]	Total elec. cost w deg. [k\$/a]	Reg. rev. w deg. [k\$/a]	Total oper. cost w deg. [k\$/a]	Oper. cost savings w deg. [k\$/a]	Annual return [%]
Ch80%	24	3479.0	0.0	3488.6	0.1	50.0	0.1	n/a	n/a	n/a	n/a	n/a
Ch80% (sep.)	24	12.5	0.0	21.1	-1.7	50.0	-3.5	n/a	n/a	n/a	n/a	n/a
ChFull	24	3479.0	0.0	3488.6	0.0	50.0	0.0	n/a	n/a	n/a	n/a	n/a
ChFull (sep.)	24	10.8	0.0	19.4	0.0	50.0	0.0	n/a	n/a	n/a	n/a	n/a
V2B	24	3429.5	0.0	3446.9	41.7	100.0	41.6	3419.4	0.0	3433.1	59.9	63.8
V2B (Stat)	24	3414.2	0.0	3429.0	64.3	130.0	45.8	3396.9	0.0	3408.8	84.0	67.1
V2X	24	3432.0	12.2	3458.3	33.2	100.0	37.2	3426.4	10.1	3436.5	55.9	58.1
V2X (Stat)	24	3419.4	18.6	3439.0	53.3	130.0	39.9	3410.9	16.0	3417.9	76.6	59.4
V2X (sep.)	24	2.8	12.9	8.1	11.1	100.0	11.6	2.3	10.7	5.6	13.3	12.8
uni-dir	24	3478.6	0.0	3488.2	0.7	50.0	1.3	3478.6	0.0	3488.2	0.7	1.3
uni-dir (sep.)	24	0.8	0.0	9.4	9.9	50.0	20.7	0.8	0.0	9.5	9.9	20.7
Ch80%	60	3478.5	0.0	3498.6	0.6	40.0	1.5	n/a	n/a	n/a	n/a	n/a
Ch80% (sep.)	60	12.0	0.0	25.5	-1.2	40.0	-3.0	n/a	n/a	n/a	n/a	n/a
ChFull	60	3479.0	0.0	3499.1	0.0	40.0	0.0	n/a	n/a	n/a	n/a	n/a
ChFull (sep.)	60	10.8	0.0	24.3	0.0	40.0	0.0	n/a	n/a	n/a	n/a	n/a
V2B	60	3399.1	0.0	3441.7	53.3	120.0	34.5	3371.2	0.0	3406.3	111.0	71.9
V2B (Stat)	60	3376.4	0.0	3416.3	86.8	165.0	46.2	3345.9	0.0	3372.2	145.6	76.7
V2X	60	3394.6	10.2	3471.0	49.2	120.0	31.9	3382.1	8.6	3413.1	99.4	66.2
V2X (Stat)	60	3370.7	7.8	3433.1	75.1	165.0	39.1	3348.3	10.4	3377.0	132.2	70.0
V2X (sep.)	60	13.2	7.7	39.8	-12.4	120.0	-6.9	8.2	5.6	22.1	2.7	2.3
uni-dir	60	3478.6	0.0	3498.7	0.7	40.0	1.2	3478.6	0.0	3498.7	0.7	1.1
uni-dir (sep.)	60	0.8	0.0	15.6	9.9	40.0	16.5	0.8	0.0	15.6	9.9	16.5

Several inputs of the controller were perfectly matched with the simulation, which in reality would always include some level of uncertainty. Examples are the perfect knowledge of weather forecast data over the next 24 h or the perfect projection of base electricity consumption over the next 24 h. Those were matched to assess the technical potential in a best-case scenario, and also because field uncertainty is not well researched and can range widely based on the used forecast methodology. However, in [47] the authors found that due to the regular updating of controller inputs, e.g., at each 5-min control timestep, and in conjunction with on-site environmental measurements, the performance impact of typical weather forecast uncertainty across U.S. on an MPC controlling a smart building was largely eliminated. Another area which is challenging for predictive control systems is the uncertain and spontaneous human behavior in the way PEVs are used in their primary function as transportation. It is therefore very challenging to develop accurate prediction models for PEV availability to provide V2X services. This study focused on U.S. military facilities where day-ahead reservations through a fleet management system are typically required. In this scenario the uncertainty of PEV availability is low, which, based on LBNL's experience with the PEV fleet operations at the LAAFB, is consistent with non-work hours and diligent use of a fleet reservation system. Also, the DOPER controller excluded all vehicles from daily V2G participation which had any associated trips during the day. This would provide additional reserves in case of unforeseen fleet demand.

The way frequency regulation participation was modeled was different than carried out during the field demonstration at LAAFB. In this study PEVs were able to individually bid any amount, given power and energy limits and overall minimum regulation requirements, and total power provided for regulation was subtracted from the site's utility meter. While this methodology is accurate in simulation, real-world deployments likely would require post-processing of utility meter data to disaggregate frequency regulation dispatch from base load demand. Load aggregators could facilitate between utilities and customers to streamline this process. Several PEV manufacturers such as Ford and Tesla already sell bi-directional charging stations and offer load aggregation services to end-users. While such expansion of the traditional automotive industry into electric power grid providers can be challenging, it also likely reduces barriers for market entry. PEV manufacturers

have the most accurate data about their drivetrain battery degradation behavior, and also can provide extended warranty when providing such services.

The participation of PEVs in dynamic ancillary service markets such as CAISO's frequency regulation is rare and usually related to research activity. One of the first demonstrations was at the LAAFB where the PEV fleet of Nissan LEAFs actively participated in the frequency regulation market for over 20 months providing a total of 255 MWh of regulation up and 118 MWh of regulation down [24]. While it is technically feasible, the trade offs for providing V2X remain uncertain. This study showed that PEV drivetrain battery temperatures, Fig. 7, significantly increased when providing V2X. While PEV drivetrain battery temperatures mostly remained within a 60 °C threshold, the larger 60 kWh battery size led to higher median temperatures than the 24 kWh one, which can be attributed to the assumption of same form factor with the 24 kWh model and equivalent exposed surfaces for heat exchange with the environment. However, it can be seen that the cases with battery degradation in the control objective have a reduced median battery temperature. In those cases the DOPER controller actively managed the expected battery temperature and associated degradation to the economical optimum between cost of battery replacement and monetary benefit from electricity cost savings and regulation revenue. While this study only considered symmetric bidding, i.e., equal bids of regulation up and down, non-symmetric bidding could increase revenue from regulation. For example instead of charging PEV batteries through the site demand, a strategic bid for regulation down could be placed. However, this strategy is risky since actual regulation dispatch is unknown which can result in a lack or excess of energy.

The active management of battery degradation led to a significant increase in battery lifetime, see Fig. 8. While the MPC (V2X) scenario without considering battery degradation shortened the battery lifetime to 2.1 years, the same scenario with active management of battery degradation increased it to 3.5 years. Combining the trade-offs in a full cost analysis, Fig. 5, it can be seen that the V2B and V2X scenarios far exceed uni-directional benefits, with annual return on investment rates of up to 66.3% for the 24 kWh battery size, and up to 106.0% for the 60 kWh, essentially resulting in a payback period of one to two years for an installation which typically lasts for more than 10 years. However, PEV drivetrain batteries will need to be replaced throughout

their life cycle. While DOPER considered the cost of replacing the battery, the associated unavailability of the vehicle, arrangement of service, etc. were not considered in this study. Given that annual ROIs for V2X are equivalent to V2B, i.e., not providing V2G service, but battery lifetime is increased by 42.8%, from 3.5 to 5.0 years, it might be more practical to only provide V2B services. However, other drivetrain systems with active battery conditioning might be able to mitigate degradation effects and therefore make V2G more attractive. Also higher prices for providing frequency regulation could change V2G participation in the future.

5. Conclusion

Plug-in electric vehicles pose a tremendous potential to reshape the way vehicles are used today. Especially PEV fleets with predictable usage patterns can provide great benefit through vehicle-to-building and vehicle-to-grid operations. While premature drivetrain battery degradation is often cited as major concern of PEV owners, this study showed that advanced control strategies can actively predict and manage battery degradation to maximize the benefits of PEVs.

Declaration of competing interest

The authors declare the following financial interests/personal relationships which may be considered as potential competing interests: Douglas R. Black reports financial support was provided by California Energy Commission.

Data availability

Data will be made available on request.

Acknowledgments

This work was supported by the U.S. Department of Energy under Contract No. DE-AC02-05CH11231. Additional support was provided by the California Energy Commission under the Electric Program Investment Charge program, solicitation number PON-13-301, that was awarded to Lawrence Berkeley National Laboratory for the work herein.

Appendix

Summary Table 5 of median results across all scenarios.

References

- [1] Ebi KL, Vanos J, Baldwin JW, Bell JE, Hondula DM, Errett NA, et al. Extreme weather and climate change: population health and health system implications. *Annu Rev Public Health* 2021;42:293.
- [2] Army US. Army climate strategy. 2022, <https://www.army.mil/>.
- [3] Donadee J, Ilic M. Stochastic optimization of grid to vehicle frequency regulation capacity bids. *IEEE Trans Smart Grid* 2014;5:1061–9.
- [4] Ansari M, Al-Awami A, Sortomme E, Abidoeric M. Coordinated bidding of ancillary services for vehicle-to-grid using fuzzy optimization. *IEEE Trans Smart Grid* 2015;6:261–70.
- [5] Yao E, Wong V, Schober R. Robust frequency regulation capacity scheduling algorithm for electric vehicles. *IEEE Trans Smart Grid* 2016;443–52.
- [6] Sortomme E, El-Sharkawi M. Optimal combined bidding of vehicle-to-grid ancillary services. *IEEE Trans Smart Grid* 2012;3:70–9.
- [7] MacDonald J, Cappers P, Callaway D, Kiliccote S. Demand response providing ancillary services: a comparison of opportunities and challenges in the US wholesale markets. In: *Proceedings of the 2012 grid interop conference*. Dec. 2012.
- [8] Bessa R, Matos M, Soares F, Lopes J. Optimized bidding of a EV aggregation agent in the electricity market. *IEEE Trans Smart Grid* 2012;443–52.
- [9] Vagropoulos SI, Bakirtzis AG. Optimal bidding strategy for electric vehicle aggregators in electricity markets. *IEEE Trans Power Syst* 2013;28:4031–41.
- [10] Shafie-khah M, Heydarian-Forushani E, Hamedani Golshan ME, Siano P, Moghadam M, Sheikholeslami M, et al. Optimal trading of plug-in electric vehicle aggregation agents in a market environment for sustainability. *Appl Energy* 2016;162:601–12.
- [11] Kaur K, Kumar N, Singh M. Coordinated power control of electric vehicles for grid frequency support: MILP-based hierarchical control design. *IEEE Trans Smart Grid* 2019.
- [12] Chen X, Leung K-C, Lam A, Hill D. Online scheduling for hierarchical vehicle-to-grid system: Design formulation, and algorithm. *IEEE Trans Veh Technol* 2019.
- [13] Janfeshan K, MAS M. Hierarchical supervisory control system for PEVs participating in frequency regulation of smart grids. *IEEE Power Energy Technol* 2017.
- [14] Liu J, Lin G, Rehtanz C, Huang S, Zhou Y, Li Y. Data-driven intelligent EV charging operating with limited chargers considering the charging demand forecasting. *Int J Electr Power Energy Syst* 2022.
- [15] Ploehn H, Ramadass P, White R. Solvent diffusion model for aging of lithium-ion battery cells. *J Electrochem Soc* 2004;A456–62.
- [16] Wang J, Purewal J, Hicks-Garner J, Soukiazian S, Sherman E, Sorenson A, et al. Degradation of lithium ion batteries employing graphite negatives and nickel-cobalt-manganese oxide + spinel manganese oxide positives: Part 1, aging mechanisms and life estimations. *J Power Sources* 2014;269:937–48.
- [17] Thompson AW. Economic implications of lithium ion battery degradation for Vehicle-to-Grid (V2X) services. *J Power Sources* 2018;396:691–709.
- [18] Wang D, Coignard J, Zeng T, Zhang C, Saxena S. Quantifying electric vehicle battery degradation from driving vs. vehicle-to-grid services. *J Power Serv* 2016;332:193–203.
- [19] Li S, Zhao P, Gu C, Li J, Cheng S, Xu M. Online battery protective energy management for energy-transportation nexus. *IEEE Trans Ind Inf* 2022;18(11):8203–12.
- [20] DeForest N, MacDonald J, Black D. Day ahead optimization of an electric vehicle fleet providing ancillary services in the Los Angeles Air Force Base vehicle-to-grid demonstration. *Appl Energy* 2018;987–1001.
- [21] Mamay C, Stadler M, Siddiqui A, DeForest N, Donadee J, Bhattacharya P, et al. Applications of optimal building energy system selection and operation. *Proc Inst Mech Eng A J Power Energy* 2013;227(1):82–93.
- [22] Mashayekh S, Stadler M, Cardoso G, Heleno M. A mixed integer linear programming approach for optimal DER portfolio, sizing, and placement in multi-energy microgrids. *Appl Energy* 2017;187.
- [23] Wenzel G, Negrete-Pincetic M, Olivares D, Macdonald J, Callaway D. Real-time charging strategies for an electric vehicle aggregator to provide ancillary services. *IEEE Trans Smart Grid* 2017;PP:1.
- [24] Black D, MacDonald J, DeForest N, Gehbauer C. Los Angeles air force base vehicle-to-grid demonstration. California Energy Commission; 2017, CEC-500-2018-025.
- [25] Gehbauer C, Mueller J, Swenson T, Vrettos E. Photovoltaic and behind-the-meter battery storage: advanced smart inverter controls and field demonstration. *Tech. Rep., Berkeley, CA (United States): Lawrence Berkeley National Laboratory*; 2021.
- [26] Smith K, Earleywine M, E. wood AP. Battery wear from disparate duty cycles: Opportunities for electric-drive vehicle battery health management. In: *Am. control conference*. 2012.
- [27] Gyan P. Calendar aging modeling of lithium-ion batteries. In: *Mat4Bat summer sch.* 2015.
- [28] Hoke A, Brissette A, Pratt A, Smith K. Electric vehicle charge optimization including effects of lithium-ion battery degradation. In: *IEEE vehicle power propulsion conference*. 2011.
- [29] Neubauer J. Battery lifetime analysis and simulation tool (BLAST) documentation. *Tech. Rep., Golden, CO (United States): National Renewable Energy Laboratory*; 2014.
- [30] Wang J, Liu P, Hicks-Garner J, Sherman E, Soukiazian S, Verbrugge M, et al. Cycle-life model for graphite LiFePO₄ cells. *J Power Sources* 2011.
- [31] Wang D, Coignard J, Zeng T, Zhang C, Saxena S. Quantifying electric vehicle battery degradation from driving vs. vehicle-to-grid services. *J Power Sources* 2016.
- [32] Ben-Marzouk M, Chaumond A, Redondo-Iglesias E, Montaru M, Pelissier S. Experimental protocols and first results of calendar and/or cycling aging study of lithium-ion batteries - the MOBICUS project. In: *29th World electr. veh. symp. exhib.* 2016.
- [33] Delaille A, Grolleau S, Duclaud F. SIMCAL Project: calendar aging results obtained on a panel of 6 commercial Li-ion cells. In: *Electrochem. energy summit*. 2013.
- [34] Gyan P, Aubret P, Hafsaoui J, Sellier F, Bourlot S, Zinola S, et al. Experimental assessment of battery cycle life within the SIMSTOCK research program. In: *Oil gas sco. technol. D lfp energies Nouv.* 2013.
- [35] Petit M, Prada E, Sauvart-Moynot V. Development of an empirical aging model for Li-ion batteries and application to assess the impact of Vehicle-to-Grid strategies on battery lifetime. *Appl Energy* 2016.
- [36] Li S, Zhao P, Gu C, Li J, Huo D, Cheng S. Aging mitigation for battery energy storage system in electric vehicles. *IEEE Trans Smart Grid* 2022;1.
- [37] Tanim T, Shirk M, Bewley R, Dufek E, Liaw B. Fast charge implications: Pack and cell analysis and comparison. *J Power Sources* 2018.
- [38] Uddin K, Jackson T, Widanage W, Chouchelamane G, Jennings P, Marco J. On the possibility of extending the lifetime of lithium-ion batteries through optimal V2G facilitated by an integrated vehicle and smart-grid system. *Energy* 2017.

- [39] Idaho National Laboratory. BEV battery testing results: 2013 Nissan leaf - VIN 0646. 2014, INL/MIS-14-31587.
- [40] Idaho National Laboratory. BEV battery testing results: 2013 Nissan leaf - VIN 9270. 2014, INL/MIS-14-31587.
- [41] Idaho National Laboratory. BEV battery testing results: 2013 Nissan leaf - VIN 5045. 2014, INL/MIS-14-31587.
- [42] Gray T, Wishart J, Shirk M. 2011 Nissan leaf VIN 0356 electric vehicle battery test results. Tech. Rep., Idaho Falls, ID (United States): Idaho National Laboratory; 2016.
- [43] Modelisar. An international standard for systems and embedded software design in vehicles. 2017, URL <https://itea4.org/project/impact-stream/modelisar-impact-story.html>.
- [44] Wattendorf K. Emporia energy partners with BREK electronics to develop bi-directional EV charger. 2022.
- [45] Denholm P, O'Connell M, Brinkman G, Jorgenson J. Overgeneration from solar energy in California. A field guide to the duck chart. Tech. Rep., Golden, CO (United States): National Renewable Energy Laboratory; 2015.
- [46] Gehbauer C, Stosic A, Black D. Synthetic caiso frequency regulation signal. In: 2020 IEEE power & energy society general meeting. IEEE; 2020, p. 1–5.
- [47] Grant P, Gehbauer C. Evaluating the impact of weather forecast inaccuracy on performance of model predictive control for dynamic facades. In: Proceedings of 2022 building performance modeling conference and SimBuild. 2022.